Journal of Molecular Structure 1059 (2014) 51–60

Contents lists available at ScienceDirect

Journal of Molecular Structure

journal homepage: www.elsevier.com/locate/molstruc

Self-catalyzed syntheses, structural characterization, DPPH radical scavenging-, cytotoxicity-, and DFT studies of phenoxyaliphatic acids of 1,8-dioxo-octahydroxanthene derivatives

G.S. Suresh Kumar [a], A. Antony Muthu Prabhu [b], P.G. Seethalashmi [c], N. Bhuvanesh [d], S. Kumaresan [e,*]

[a] Faculty of Chemistry, Department of Science and Humanities, Dr. Mahalingam College of Engineering and Technology (Dr. MCET), Udumalai Road, Pollachi 642 003, Tamil Nadu, India
[b] Department of Chemistry, Manonmaniam Sundaranar University, Tirunelveli 627 012, Tamil Nadu, India
[c] Department of Chemistry, A.P.C. Mahalaxmi College for Women, Thoothukudi 628 002, Tamil Nadu, India
[d] Department of Chemistry, Texas A & M University, College Station, TX 77842, USA
[e] Department of Chemistry, Noorul Islam University, Kumaracoil, Thuckalai 629 180, Tamil Nadu, India

HIGHLIGHTS

- Phenoxyaliphatic acids act as self-catalysts for the syntheses of xanthenes.
- Xanthene **2a** has better radical scavenging- and anticancer activities.
- DFT studies confirm the stabilization through intermolecular H-bonding.
- Compound **2c** has the highest energy gap, highest hardness, and lowest softness.
- Self-catalyzed formation of **2a** is proved by experimental and DFT studies.

GRAPHICAL ABSTRACT

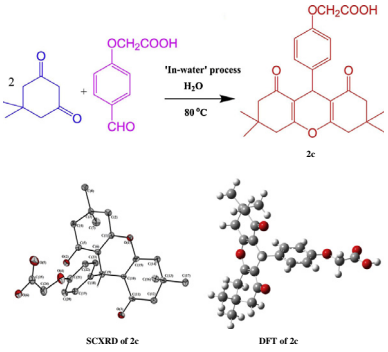

ARTICLE INFO

Article history:
Received 29 August 2013
Received in revised form 6 November 2013
Accepted 6 November 2013
Available online 16 November 2013

Keywords:
Xanthenes
Formylphenoxyaliphatic acids
DPPH radical scavenging
DFT studies

ABSTRACT

One-pot, in-water syntheses of phenoxyaliphatic acids of 1,8-dioxo-octahydroxanthene derived from dimedone and formylphenoxyaliphatic acids are reported. Geometries of compounds **2b**, **2c**, and **5a** have been examined crystallographically. The synthesized compounds showed better DPPH radical scavenging activity and cytotoxicity against A431 cancer cell line. The molecular properties of all synthesized xanthenes have been investigated using single crystal XRD and DFT method. Self-catalyzed Bronsted–Lowry acid catalytic behavior was also investigated by both experimental and theoretical methods.

1. Introduction

Density Functional Theory (DFT) finds increasing use in applications related to biological systems. The calculation of a wide range of molecular properties with DFT provides a close relationship between theory and experiment. This usually leads to important clues about the geometric, electronic, and spectroscopic properties of the systems concerned. Advancements in methodology and implementations have reached a point where predicted properties of reasonable to high quality can be obtained [1]. B3LYP/3-21G(d) method has been successfully used to predict the geometry and electronic structure of a molecule due to its more advantages [2].

* Corresponding author. Tel.: +91 94431 82502.
E-mail address: skumarmsu@yahoo.com (S. Kumaresan).

0022-2860/$ - see front matter © 2013 Elsevier B.V. All rights reserved.
http://dx.doi.org/10.1016/j.molstruc.2013.11.016

Xanthenes have received more attention due to their bioactivities against human pathogens [3]. They exhibit antifungal-, antiviral-, antibacterial-, anti-inflammatory, etc. activity [4]. Furthermore, xanthenes are used in dyes, laser technologies, and fluorescent materials for visualization of biomolecules [5]. Due to the versatile application possibilities of xanthenes, there is a continuous exploration for the formulation of newer synthetic entities *via* efficient methods. Phenoxyaliphatic acid derivatives possess a wide range of diverse bioactivities such as anti-inflammatory, antioxidant, antibacterial, analgesic, antisickling, antipaemic, antiplatelet, DPPH radical scavenging, DNA protection, non-prostanoid prostacyclin mimetic, diuretic, and growth regulatory [6].

Water finds an important role in organic syntheses as solvent because of its abundance and less toxicity. Based on the solubility of starting materials in water and reaction conditions, water-mediated reactions are classified either as 'in-water' process or 'on-water' process [7,8].

Syntheses of xanthenes from dimedone and aromatic aldehyde(s) using Bronsted–Lowry acid catalysts have been reported earlier [9]. To the best of our knowledge, we have not encountered any report regarding the use of aromatic aldehydes bearing carboxylic acid group in the side chain for the formation of 1,8-dioxo-octahydroxanthenes. This mooted us to carry the one-pot syntheses of 1,8-dioxo-octahydroxanthenes from dimedone and formylphenoxyacetic acid(s) at elevated temperature in water without any external acid catalyst. In the present study, we have prepared different xanthene derivatives making use of the inherent self catalyzing capacity of the carboxylic acid group present in the phenoxyaliphatic acids. DPPH radical scavenging activity, cytotoxicity, and molecular properties of the newly synthesized compounds were studied by single crystal XRD and DFT methods.

2. Experimental

2.1. General

Phenoxyaliphatic acids [10] and their corresponding esters [11] were synthesized as per the reported methods. Melting points were measured in open capillary tubes and are uncorrected. Infrared spectra were recorded on a JASCO FT-IR Model 410 spectrophotometer (KBr disc). Band positions are reported in reciprocal centimetres (cm^{-1}). The ^1H NMR and ^{13}C NMR spectra were recorded on a Bruker (Avance) 300 MHz NMR instrument using TMS as internal standard and $CDCl_3$ as solvent. The electrospray mass spectra were recorded on a THERMO Finnigan LCQ Advantage max ion trap mass spectrometer. Samples (10 μL) (dissolved in solvent such as methanol/acetonitrile/water) were introduced into the ESI source through Finnigan surveyor autosampler. Elemental analyses were performed on a Perkin Elmer 2400 Series II Elemental CHNS analyzer. Silica gel-G plates (Merck) were used for TLC analysis with a mixture of hexanes and ethyl acetate as eluent.

2.2. General synthesis of phenoxyaliphatic acids of xanthene

Formylphenoxyaliphatic acid (1 equi.) was dissolved in water (10 mL) at 80 °C and dimedone (2 equi.) was added with vigorous stirring. After 10 min, the reaction mixture was cooled to room temperature, the solid was filtered, washed with water, dried well, and recrystallized from hot ethanol.

2.2.1. 2-[2-(3,3,6,6-Tetramethyl-1,8-dioxo-2,3,4,5,6,7,8,9-octahydro-1H-xanthen-9-yl)phenoxy]acetic acid (**2a**)

Pale yellow solid, 82%, m.p. 206–208 °C; ^1H NMR (300 MHz, δ ppm): 0.99 (s, 6H), 1.11 (s, 6H), 2.21 (s, 4H), 2.49 (s, 4H), 4.85 (s, 2H), 5.20 (s, 1H), 6.63 (d, J = 8.7 Hz, 1H), 6.89 (t, J = 7.5 Hz, 1H), 6.96 (d, J = 7.5 Hz, 1H), 7.11 (t, J = 7.8 Hz, 1H); ^{13}C NMR (75 MHz, δ ppm): 18.7, 21.7, 23.6, 26.7, 35.3, 45.1, 59.9, 105.1, 110.1, 116.6, 122.5, 123.5, 127.6, 147.7, 157.9, 164.5, 191.9; IR (KBr, ν, cm^{-1}): 1756, 1664; ESI MS: m/z (M + H) 425.0. Anal.Calcd. for $C_{25}H_{28}O_6$: C, 70.74; H, 6.65%. Found: C, 70.72; H, 6.68%.

2.2.2. 2-(2-methoxy-6-(3,3,6,6-tetramethyl-1,8-dioxo-2,3,4,5,6,7,8,9-octahydro-1H-xanthen-9-yl)phenoxy)acetic acid (**2b**)

Pale yellow solid, 84%, m.p. 221–223 °C; ^1H NMR (300 MHz, δ ppm): 0.97 (s, 6H), 1.08 (s, 6H), 2.14 (dd, 4H), 2.49 (s, 4H), 3.78 (s, 3H), 4.67 (s, 2H), 4.99 (s, 1H), 6.64 (d, J = 7.3 Hz, 1H), 6.74 (d, J = 7.8 Hz, 1H), 6.88 (t, J = 7.8 Hz, 1H); ESI MS: m/z (M-H) 453.4; Anal.Calcd. for $C_{26}H_{30}O_7$: C, 68.71; H, 6.65%. Found: C, 68.76; H, 6.69%.

2.2.3. 2-[4-(3,3,6,6-Tetramethyl-1,8-dioxo-2,3,4,5,6,7,8,9-octahydro-1H-xanthen-9-yl)phenoxy]acetic acid (**2c**)

Pale yellow solid, 80%, m.p. 210–212 °C; ^1H NMR (300 MHz, δ ppm): 0.99 (s, 6H), 1.11 (s, 6H), 2.00 (s, 4H), 2.46 (s, 4H), 4.75 (s, 2H), 5.30 (s, 1H), 7.24 (m, 4H); IR (KBr, cm^{-1}): 1758, 1662; ESI MS: m/z (M + H) 425.0; Anal.Calcd. for $C_{25}H_{28}O_6$: C, 70.74; H, 6.65%. Found: C, 70.76; H, 6.69%.

2.2.4. 3,3,6,6-Tetramethyl-9-phenyl-3,4,5,6,7,9-hexahydro-1H-xanthene-1,8(2H)-dione (**5a**)

Pale yellow solid, m.p. 188–190 °C, 86%, ^1H NMR (300 MHz, δ ppm): 0.99 (s, 6H), 1.10 (s, 6H), 2.20 (4H), 2.67 (s, 4H), 4.75 (s, 1H), 7.12 (d, J = 7.5 Hz, 1H), 7.21 (t, J = 7.2 Hz, 2H), 7.27 (d, J = 8.1 Hz, 2H); Anal.Calcd. for $C_{23}H_{26}O_3$: C, 78.83; H, 7.48%; Found: C, 78.80; H, 7.44.

2.2.5. Ethyl 2-[2-(3,3,6,6-tetramethyl-1,8-dioxo-2,3,4,5,6,7,8,9-octahydro-1H-xanthen-9-yl)phenoxy]acetate (**5b**)

Yellow solid, 82%, m.p. 178–180 °C; ^1H NMR (300 MHz, δ ppm): 0.97 (s, 6H), 1.08 (s, 6H), 1.29 (t, J = 7.0 Hz, 3H), 2.17 (s, 2H), 2.53 (s, 2H), 4.25 (q, J = 6.9 Hz, 2H), 4.54 (s, 2H), 4.87 (s, 1H), 6.63 (d, J = 8.1 Hz, 1H), 6.91 (t, J = 7.5 Hz, 1H), 7.09 (t, J = 7.5 Hz, 1H), 7.68 (d, J = 8.1 Hz, 1H); ^{13}C NMR (75 MHz, δ ppm): 14.0, 27.1, 29.0, 29.9, 31.8, 40.7, 50.6, 60.8, 65.9, 111.5, 113.3, 121.2, 127.6, 130.7, 132.6, 156.0, 162.7, 168.4, 196.4; IR (KBr, cm^{-1}): 1762, 1662; ESI MS: m/z (M + H) 453.0; Anal.Calcd. for $C_{27}H_{32}O_6$: C, 71.66; H, 7.13%; Found: C, 71.62; H, 7.16%.

2.3. Single crystal XRD

The crystal structures were determined using a BRUKER APEX 2 X-ray (three-circle) diffractometer. The data reduction was done with the program APEX2 [12]. The absorption correction was employed using the program SADABS [13]. The structure solution was obtained using SHELXTL (XS) [14] and refined on F^2 to convergence [14,15]. Absence of additional symmetry was verified using PLATON (ADDSYM) [16]. Powder X-ray diffraction data were recorded at room temperature using XPERT-PRO diffractometer system with $CuK_{\alpha1}$, $CuK_{\alpha2}$, and CuK_{β} with radiation of wavelength 1.54060, 1.54443, and 1.39225 Å respectively.

2.4. DPPH radical scavenging assay

The radical scavenging activity of the compounds was evaluated as per the method of Blois [17] with a slight modification [18]. The compounds (**2a–c**, **5b**) and BHA at different concentrations (25, 50, 75, and 100 ppm in 1 mL) were taken in different test tubes. Four milliliters of 0.1 mM methanolic solution of DPPH was added to these tubes and shaken vigorously. The tubes were allowed to stand at 27 °C for 20 min. The control was prepared as above in

the absence of any compound and methanol was used for the baseline correction. Optical density (OD) of the samples was measured at 517 nm. Radical scavenging activity was expressed as the inhibition percentage and was calculated using the following formula:

% Radical scavenging activity = (Control OD – Sample OD/Control OD) ×100.

2.5. In vitro anticancer activity

The human skin epithelial cell carcinoma cell line (A431), human stomach adenocarcinoma cancer cell line (AGS), and glioblastoma cell line (U373MG) were obtained from National Centre for Cell Science (NCCS), Pune and grown in Dulbecco's Modified Eagle's Medium (DMEM) containing 10% fetal bovine serum (FBS). All cells were maintained at 37 °C, 5% CO_2, 95% air, and 100% relative humidity. Maintenance cultures were passaged weekly and the culture medium was changed twice a week [19].

2.5.1. Cell treatment procedure

The monolayer cells were detached with trypsin-ethylenediaminetetraacetic acid (EDTA) to make single cell suspensions and the viable cells were counted using a hemocytometer and diluted with a medium containing 5% FBS to a give final density of 1×10^5 cells/mL. One hundred microlitres per well of cell suspension were seeded into 96-well plates at a plating density of 10,000 cells/well and incubated to allow for cell attachment at 37 °C, 5% CO_2, 95% air, and 100% relative humidity. After 24 h, the cells were treated with serial concentrations of the extracts and fractions. They were initially dissolved in DMSO and further diluted in serum free medium to produce five concentrations. One hundred microlitres per well of each concentration was added to plates to obtain final concentrations of 300, 150, 75, 37.5, and 18.75 μM. The final volume in each well was 200 μL and the plates were incubated at 37 °C, 5% CO_2, 95% air and 100% relative humidity for 48 h. The medium without samples served as control. Triplicate was maintained for all concentrations.

2.5.2. MTT assay

MTT is a yellow water soluble tetrazolium salt. A mitochondrial enzyme in living cells, succinate-dehydrogenase, cleaves the tetrazolium ring, converting the MTT to an insoluble purple formazan. The amount of formazan produced is directly proportional to the number of viable cells. After 48 h of incubation, 15 μL of MTT (5 mg/mL) in phosphate buffered saline (PBS) was added to each well and incubated at 37 °C for 4 h. The medium with MTT was then flicked off and the formazan crystals formed were solubilized in 100 μL of DMSO and the absorbance was measured at 570 nm using a microplate reader. The % cell inhibition was determined using the following formula.

% Cell inhibition = 100 – Abs (sample)/Abs (control) ×100.

Nonlinear regression graph was plotted between % cell inhibition and $\log_{10}$ concentration and IC_{50} was determined using GraphPad Prism software.

2.6. Computational methodology

The theoretical energy calculation of xanthenes in gas phase was performed using the analytical gradient method of DFT with Becke's three parameters (B3) exchange functional together with the Lee–Yang–Parr (LYP) non-local correlation functional, symbolized B3LYP [20] by means of 3-21G (d) basis set implemented in Gaussian 09 W software package [21]. The electronic properties were calculated from both the Koopmans' theorem (orbital energy consideration represented by subscript O) and the total energies denoted with subscript E of the species as follows: the ionization potential is calculated as the energy differences between the energy of the compound derived from electron-transfer (radical cation) and the respective neutral compound; $IP_E = E_{cation} - E_n$; $IP_o = -E_{HOMO}$, the electron affinity is computed as the energy differences between the neutral molecule and the anion molecule: $EA = E_n - E_{anion}$; $EA_o = -E_{LUMO}$, respectively. From these calculations the other parameters such as electronegativity (χ), electrochemical potential (μ), hardness (η), softness (σ), and electrophilicity index (ω) have been calculated [22–25].

3. Results and discussion

3.1. Syntheses of phenoxyaliphatic acids of xanthenes

We studied the model reaction for the synthesis of 2-[2-{(3,4,6,7-tetrahydro-3,3,6,6-tetramethylxanthen-1,8-dione-2-yl)methyl}phenoxy]acetic acid (**2a**) derived from dimedone (5 mmole) and 2-formylphenoxyacetic acid (2.5 mmole).

Experiments were carried out in various solvents like hexanes, benzene, toluene, acetonitrile, DMF, ethanol, aqueous ethanol (1:1), and water. The reactions did not proceed in hexanes, benzene, and toluene, but scarcely proceeded in acetonitrile, DMF, and ethanol to give 2-[2-{bis(4,4-dimethyl-2,6-dioxocyclohexyl)methyl}phenoxy]acetic acid (**4c**) (*vide* Supporting information). In the case of aqueous ethanol as solvent, both **2a** (15%) and **4c** (42%) were observed. In aqueous medium, the reaction afforded **2a** (78%). Subsequently, further optimization of the reaction conditions, including reaction temperature, reaction time, and volume of water was investigated. Satisfyingly, after a series of experiments, water was proved to be the best solvent and the yield of **2a** reached 82% when the reaction was performed in water (10 mL for 5 mmole) at 80 °C for 10 min (Scheme 1). Both starting materials were miscible at 80 °C. After 10 min, the product **2a** was thrown out from the clear solution. Thus, this reaction seems to occur *via* 'in-water process' [8].

The pH of the reaction mixture was monitored at 5.84. This manifests the formation of hydronium ion from 2-formylphenoxyacetic acid (pK_a 3.04) in water during the reaction (Fig. 1). Cyclodehydration was ensued in a single step (Fig. 1). Earlier reports confirmed the need for an acid or a base as catalyst for the cyclodehydration [9,26].

Carboxylic ester aldehyde (**3b**) and sodium salt of acid aldehyde (**3c**) were used to prove the essentiality of the carboxylic acid group for the reaction to go (*vide* Supporting information for the evidence for self-catalyzed in-water reaction). Both ethyl 2-(2-formylphenoxy)acetate (**3b**) and sodium salt of 2-formylphenoxyacetic acid (**3c**) behaved similar to benzaldehyde (**3a**) [26].

From one-pot syntheses of xanthenes (**2a**, **5a**, and **5b**) (*vide* Supporting information, Scheme s1), it is believed that the carboxylic acid group in 2-formylphenoxyacetic acid behaves as a Bronsted–Lowry acid catalyst in water [27] affording **2a** (Fig. 1). Based on this, we proposed a reasonable reaction mechanism for the synthesis of **2a** through 'in-water' process (Fig. 1). We extended the same

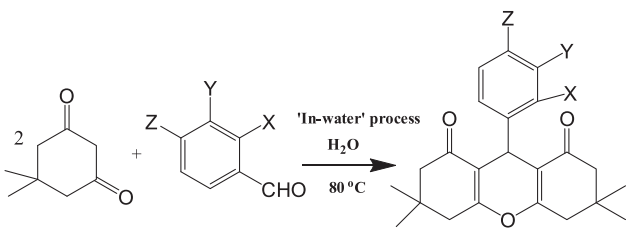

1a. X = -OCH_2COOH, Y=H, Z=H
1b. X = -OCH_2COOH, Y=-OCH_3, Z=H
1c. X = H, Y=H, Z= -OCH_2COOH

2a. X = -OCH_2COOH, Y=H, Z=H
2b. X = -OCH_2COOH, Y=-OCH_3, Z=H
2c. X = H, Y=H, Z= -OCH_2COOH

Scheme 1. Synthesis of **2** from dimedone and formylphenoxyacetic acids.

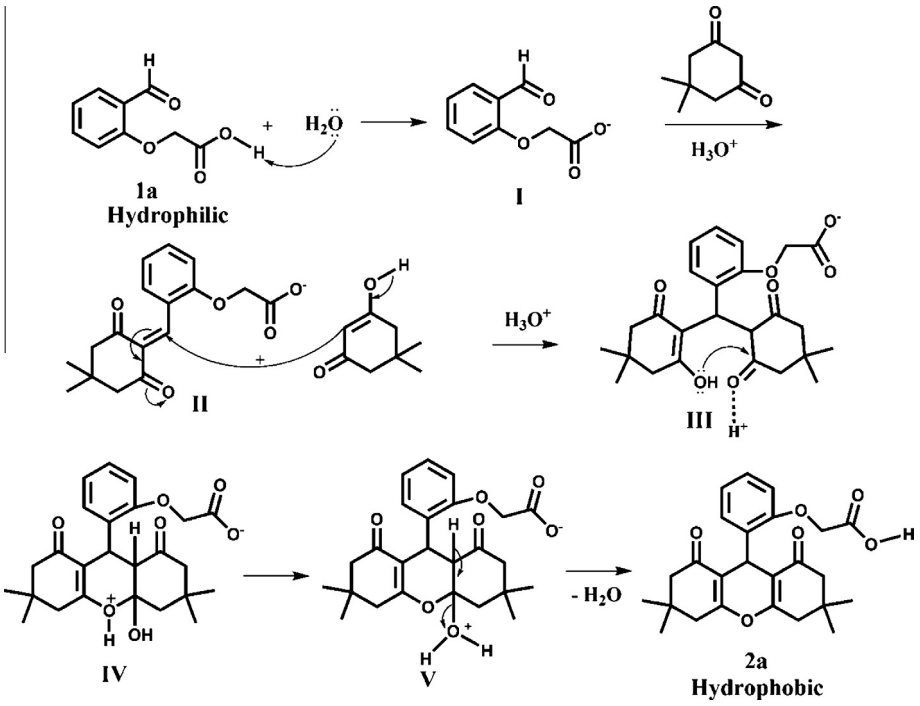

Fig. 1. Synthesis of **2a** through 'in-water' process.

condition for the syntheses of xanthenes **2b** and **2c** from 2-(2-formyl-6-methoxyphenoxy)acetic acid (**1b**) and 4-formylphenoxyacetic acid (**1c**) with dimedone. The newly synthesized compounds **2a**, **2b**, **2c**, and **5b** were characterized by single crystal XRD, IR, NMR, and mass analysis.

3.2. Single crystal XRD studies

Compounds **2b** and **2c** were crystallized using aqueous ethanol (1:1 v/v) and compound **5b** was crystallized using ethanol under slow evaporation. These compounds have been characterized by single crystal X-ray diffraction studies. The ORTEP views of the compounds **2b**, **2c**, and **5b** are shown in Fig. 2. The crystallographic data and structural refinement details for the compounds **2b**, **2c**, and **5b** are given in Table 1.

Systematic reflection conditions and statistical tests of the data suggested that the compound **2b** was crystallized as **2b·H$_2$O**. It has a centrosymmetric space group $P2_1/c$. In the crystal lattice, two molecules of **2b** are joined together through two water molecules by intermolecular hydrogen bonding. Hydrogen bonding is formed between H-atom of carboxyl group and O-atom of water molecule. The C–O bond lengths [C26–O6: 1.212 Å, C26–O7: 1.321 Å] indicate that the acid moiety is present as –COOH. The different types of hydrogen bonding present in this crystal are O7–H7···O20(w), O20(w)–H20A(w)···O2, and O20(w)–H20B(w)···O2. Carbonyl oxygen forms bifurcated hydrogen bonding with two water molecules. Two molecules of the compound **2b** are connected together through two water molecules by three types of hydrogen bondings with Etter's graph set [28] notation $R^2_2(13)$. In the formation of the dimer, a square ring with graph set designation $R^2_4(8)$ is produced (Fig. 3).

The crystal structure of **2c** shows that the molecules are self-associated. An intermolecular hydrogen bonding motif O6–H6···O2 is observed between the carboxyl group of one molecule and the carbonyl oxygen of another molecule. The C–O bond lengths [C25–O6: 1.328 Å, C25–O5: 1.197 Å] indicate that the acid moiety is present as –COOH. These molecules are connected through O6–H6···O2 hydrogen bonding with Etter's graph set [28] designator $C^1_1(13)$ forming a one dimensional zig-zag chain (Figs. 4 and 5). The O6–H6···O2 bond distance is 2.623 Å which is nearly linear with an angle of 169.99°.

In compound **5b**, O6–C26–C27 group is found to be disordered and successfully modeled in two positions. Only one position of the ORTEP diagram is shown for clarity [Fig. 2(c)]. Compound **5b** is stabilized by short contacts without any H-bonding. Compounds **2c** and **5b** have C–H···π interactions. The crystal structures of **2b**, **2c**, and **5b** do not exhibit any π–π stacking force.

3.3. DPPH radical scavenging activity

The role of antioxidants is their interaction with oxidative free radicals. The free radical scavenging activity of the compounds **2a**–**c** and **5b** was tested using DPPH model system [17,18] and the results are presented in Table 2. It reveals that at 25 ppm concentration, **2a** has better scavenging activity (72.46 ± 3.84) followed by **2c**. Ester **5b** has lower scavenging activity than its corresponding acid **2a**.

3.4. In vitro anticancer activity

We screened the growth inhibition or antiproliferative effects of **2a**–**c** and **5b** on the cancer cell lines A431, AGS, and U373MG following MTT assay [19]. These xanthenes have IC_{50} more than 300 μM on AGS and U373MG cell line. Table 3 reveals that **2a** has lower IC_{50} (128.2) than other derivatives on A431 cell line (*vide* Supporting information for the growth inhibition effect of **2a** on the cancer cell line A431).

3.5. Theoretical studies using DFT method

Gas phase geometry optimizations were performed starting from the crystal structure **2b·H$_2$O**, **2c**, and **5b** at the B3LYP/3-21G(d) level of theory [21]. The calculated and experimental values of the selected geometrical parameters of **5b** are given in Table 4. The calculated geometrical parameter represents good correlation

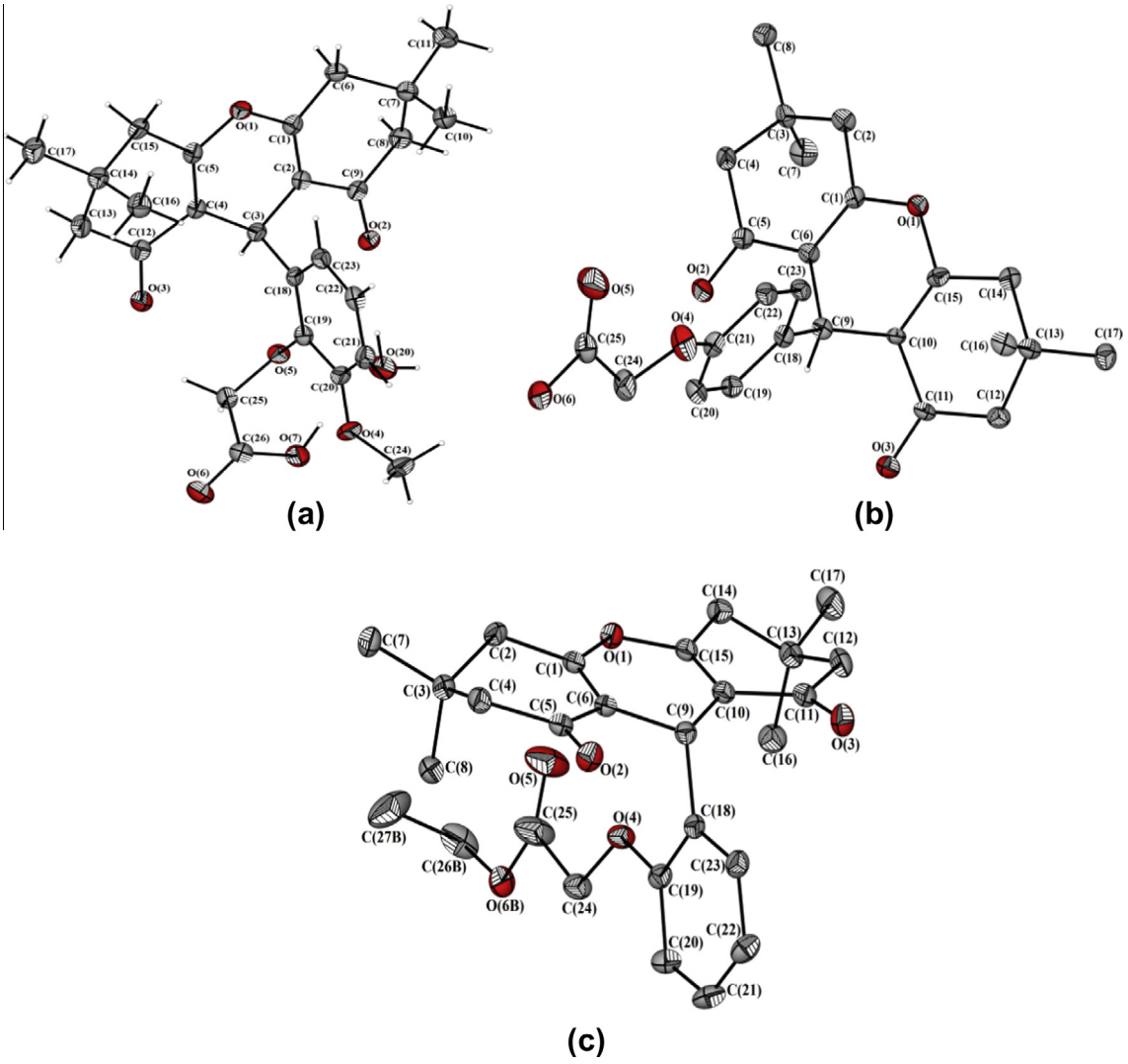

Fig. 2. ORTEP view of (a) **2b·H$_2$O**, (b) **2c**, and (c) **5b**.

Table 1
Crystal data and structure refinement of **2b·H$_2$O**, **2c**, and **5b**.

	2b·H$_2$O	**2c**	**5b**
CCDC no.	882629	875572	875479
Empirical formula	$C_{26}H_{32}O_8$	$C_{25}H_{28}O_6$	$C_{27}H_{32}O_6$
Formula weight	472.52	424.47	452.53
Appearance	Colourless block	Colourless thin plate	Colourless thin plate
Crystal size (mm^3)	0.40 × 0.32 × 0.16	0.10 × 0.07 × 0.01	0.20 × 0.16 × 0.14
Wavelength (Å)	0.71073 Å	1.54178 Å	0.71073 Å
Crystal system	Monoclinic	Orthorhombic	Monoclinic
Space group	$P2_1/c$	Pna2(1)	P2(1)/c
Unit cell dimensions	a = 10.2999(18) Å	a = 19.5079(17) Å	a = 9.6070(11) Å
	b = 17.749(3) Å	b = 5.9111(6) Å	b = 23.486(3) Å
	c = 13.256(2) Å	c = 18.7710(17) Å	c = 11.1112(13) Å
	$\alpha = \gamma = 90°$	$\alpha = \beta = \gamma = 90°$	$\alpha = \gamma = 90°$
	β = 100.370(2)°		β = 109.8120(10)°
Volume	2383.8(7) Å3	2164.5(3) Å3	2358.6(5) Å3
Z	4	4	4
Density (calculated)	1.317 Mg/m3	1.303 Mg/m3	1.274 Mg/m3
Absorption coefficient	0.097 mm^{-1}	0.756 mm^{-1}	0.089 mm^{-1}
F(000)	1008	904	968
Theta range for data collection	2.29–27.49°	4.53–60.00°	2.25–27.46°
Goodness-of-fit on $F2$	1.044	1.039	1.052
Final R indices [$I > 2$sigma(I)]	R1 = 0.0457, wR2 = 0.1164	R1 = 0.0549, wR2 = 0.1430	R1 = 0.0406, wR2 = 0.0996
R indices (all data)	R1 = 0.0743, wR2 = 0.1343	R1 = 0.0648, wR2 = 0.1503	R1 = 0.0536, wR2 = 0.1095
Largest diff. peak and hole	0.259 and −0.265 e Å−3	0.244 and −0.289 e.Å−3	0.445 and −0.366 e.Å^{-3}

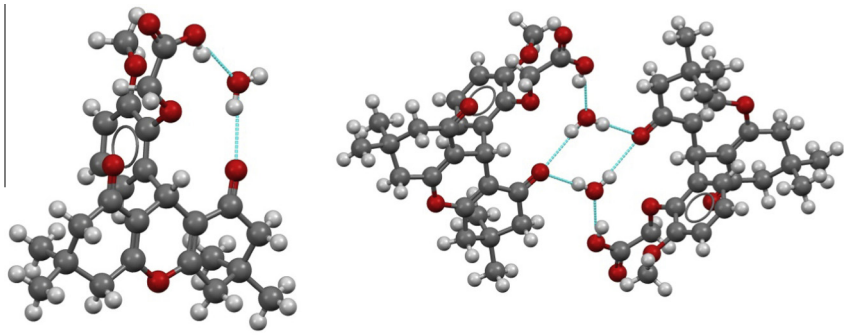

Fig. 3. H-bonding pattern for **2b**.

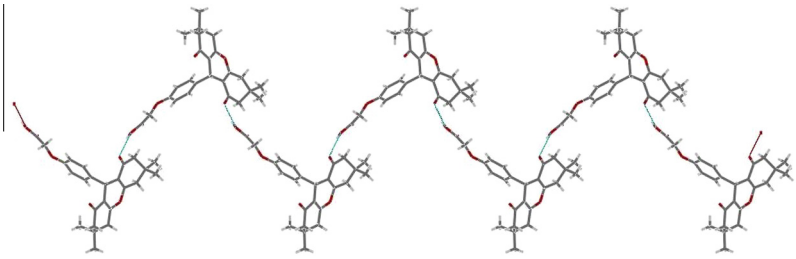

Fig. 4. H-bonding pattern for **2c** in 1D zig-zag chain.

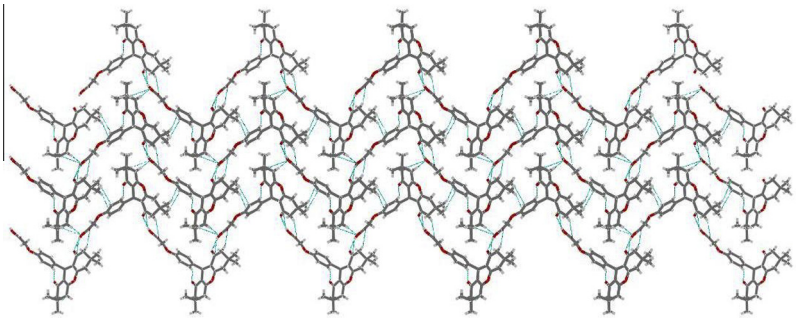

Fig. 5. 2D view for **2c** along *b* axis.

Table 2
DPPH radical scavenging activity of **2a–c** and **5b**.

Samples	% Radical scavenging activity at different concentrations (ppm)			
	25	50	75	100
2a	72.46 ± 3.84	73.76 ± 8.27	77.73 ± 1.32	79.23 ± 1.53
2b	60.49 ± 2.26	61.04 ± 5.13	63.98 ± 3.62	61.95 ± 2.54
2c	61.84 ± 0.83	62.23 ± 4.41	68.87 ± 1.48	67.04 ± 1.66
5b	42.88 ± 4.20	44.76 ± 8.68	46.07 ± 8.42	49.91 ± 6.93
BHA	93.81 ± 0.01	90.85 ± 0.89	96.58 ± 0.19	95.04 ± 0.13

Table 3
Calculation of IC_{50} using % growth inhibition against $\log_{10}$ concentration (μM) for A431 cell line.

Compounds	**2a**	**2b**	**2c**	**5b**
IC_{50} (μM)	128.2	258.4	288.4	>300

with experimental values which can germ into the calculation of the other parameters for the compound **5b**.

Similarly the ground state geometrical optimization was done on **2b·H$_2$O** and **2c**. The theoretical parameters were found to be nearly the same as the experimental parameters (Table 4). Our previous work disclosed that the *ortho*- substituted phenoxyaliphatic acid derivatives were stabilized through water molecule [6b,18b]. So we used the same DFT method for the geometrical optimization [29] of the molecule **2a** and its monohydrate (**2a·H$_2$O**). The optimized structures of **2a**, **2b**, **2c**, and **5b** are shown in Fig. 6 (*vide* Supporting information, **2a·H$_2$O** and **2b·H$_2$O**).

Table 5 reveals the total energies, frontier molecular orbital energies, and dipole moments of the compounds in gas phase. The obtained total energy values are −886730.54 kcal/mol for **2a**, −934439.46 kcal/mol for **2a·H$_2$O**, −958204.43 kcal/mol for **2b**, −1005909.46 kcal/mol for **2b·H$_2$O**, −886727.59 kcal/mol for **2c** and −935805.04 kcal/mol for **5b**. The total energy difference of the hydrated xanthenes (**2a·H$_2$O** and **2b·H$_2$O**) and their parent compounds (**2a** and **2b**) is 47707 kcal/mol. The geometry of O2 and H7···O7 groups in **2b·H$_2$O** helps accommodating a water mol-

Table 4
Selected bond lengths and bond angles of **2b·H$_2$O**, **2b**, **2c**, and **5b**.

2b·H$_2$O			**2b**	**2c**			**5b**		
Bond	XRD data	DFT data	DFT Data	Bond	XRD data	DFT data	Bond	XRD data	DFT Data
Bond length (Å)									
C1–C2	1.344(2)	1.344	1.344	C1–C6	1.355(5)	1.343	C1–C6	1.340(17)	1.343
C4–C5	1.331(2)	1.341	1.341	C10–C15	1.347(6)	1.342	C10–C15	1.340(18)	1.341
C2–C3	1.513(2)	1.517	1.514	C9–C10	1.503(5)	1.513	C6–C9	1.511(17)	1.515
C3–C4	1.511(2)	1.515	1.513	C6–C9	1.509(5)	1.518	C9–C10	1.511(17)	1.515
C3–H3	1.000	1.092	1.091	C9–H9A	1.000	1.094	C9–H9A	1.000	1.094
C9–O2	1.230(18)	1.243	1.246	C5–O2	1.244(5)	1.243	C5–O2	1.225(15)	1.242
C12–O3	1.222 (19)	1.240	1.242	C11–O3	1.232(5)	1.240	C11–O3	1.222(16)	1.243
C26–O6	1.212(2)	1.222	1.236	C25–O5	1.197(6)	1.216	C25–O5	1.188(19)	1.226
C26–O7	1.321(2)	1.363	1.334	C25–O6	1.329(5)	1.385	C25–O6A	1.413(2)	1.494
O7–H7	0.840	1.007	1.063	O6–H6	0.850	0.997	C25–O6B	1.392(3)	–
Bond angle (°)									
C6–C7–C8	107.33(13)	108.23	108.18	C2–C3–C4	107.9(3)	108.3	C2–C3–C4	108.93(10)	108.20
C13–C14–C15	108.16(13)	108.04	108.32	C12–C13–C14	107.9(3)	108.4	C12–C13–C14	111.77(11)	108.16
C1–O1–C5	118.11(12)	118.16	118.36	C1–O1–C15	118.2(3)	117.8	C1–O1–C15	118.22(10)	117.97
C2–C3–C4	108.96(13)	110.18	110.53	C6–C9–C10	108.6(3)	109.8	C6–C9–C10	109.02(10)	109.93
C2–C9–C8	118.39(13)	116.03	116.43	C6–C5–C4	118.5(3)	116.2	C6–C5–C4	118.70(11)	116.16
C4–C12–C13	117.64(14)	116.03	115.94	C10–C11–C12	118.3(3)	116.1	C10–C11–C12	118.22(11)	116.07
C18–C3–H3	109.20	106.79	107.12	C18–C9–H9A	109.0	107.8	C18–C9–H9A	107.3	106.59
O6–C26–O7	121.06(16)	123.70	123.17	O5–C25–O6	125.3(4)	123.9	O5–C25–O6A	123.53(17)	124.25
C26–O7–H7	109.50	105.78	117.18	C25–O6–H6	113.3	108.6	O5–C25–O6B	120.77(17)	
C20–O4–C24	116.06(13)	118.78	120.86	C21–O4–C24	119.5(3)	118.1			
C19–O5–C25	114.86(12)	116.20	118.18						

ecule through H-bonding for further stabilization. This is supported by DFT studies (Table 4).

3.5.1. Molecular Electrostatic Potential (MEP)

Molecular Electrostatic Potential (MEP) of **2a·H$_2$O**, **2b·H$_2$O**, **2c**, and **5b** was determined using the same DFT method (*vide* Supporting information, **2a·H$_2$O**, **2c**, and **5b**). The different values of the electrostatic potential at the surface are represented by different colours [30]. In the case of **2b·H$_2$O** (Fig. 7), the negative region (red) is localized on the carbonyl oxygen (O2), phenoxy oxygen (O5) and oxygen from water (O20) with a minimum value of −0.09031 a.u. However, the positive region (light blue) is localized on the carboxylic acid hydrogen (H7) and the H atoms H20A and H20B of water with a maximum value of 0.06061 a.u. The green region represents segments of zero potential.

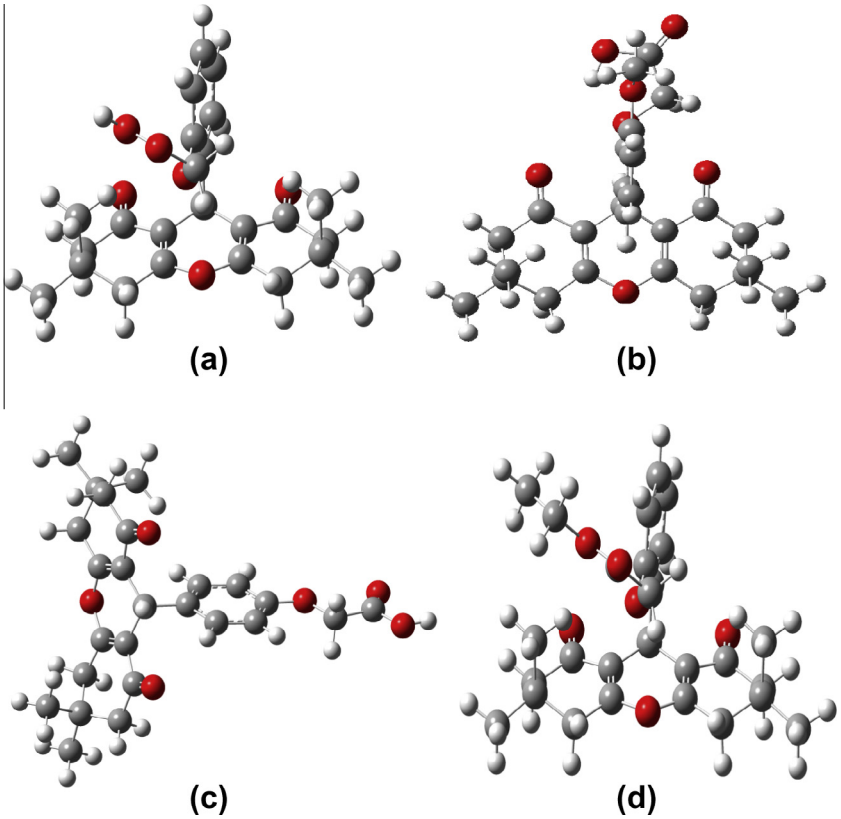

Fig. 6. Optimized structures of (a) **2a**, (b) **2b**, (c) **2c**, and (d) **5b**.

Table 5
Some molecular properties of xanthenes calculated using DFT at the B3LYP/3-21G(d) basis set in gaseous phase.

Entry	Total energy (kcal/mol)	E_{HOMO} (eV)	E_{LUMO} (eV)	ΔE (eV)	Dipole moment (Debye)	I (eV)	A (eV)	χ (eV)	μ (eV)	η (eV)	σ (eV)	ω (eV)
2a	−886730.54	−6.1271	−1.4364	4.6907	4.9442	6.1271	1.4364	3.7817	−3.7817	2.3453	0.4264	3.0489
2a·H$_2$O	−934439.46	−6.5356	−2.0554	4.4802	12.9432	6.5356	2.0554	4.2955	−4.2955	2.2401	0.4464	4.1184
2b	−958204.43	−5.9535	−1.7585	4.1950	10.3698	5.9535	1.7585	3.8560	−3.8560	2.0975	0.4767	3.5444
2b·H$_2$O	−1005909.46	−5.5620	−1.9420	3.6200	11.9313	5.5620	1.9420	3.7520	−3.7520	1.8100	0.5525	3.8888
2c	−886727.59	−6.3756	−1.5602	4.8154	4.1523	6.3756	1.5602	3.9679	−3.9679	2.4077	0.4153	3.2695
5b	−935805.04	−5.8964	−1.4214	4.4750	4.6925	5.8964	1.4214	3.6589	−3.6589	2.2375	0.4469	2.9916

I – ionization potential; A – electron affinity; χ – electronegativity; μ – electrochemical potential; η – absolute hardness; σ – softness; ω – nucleophilicity.

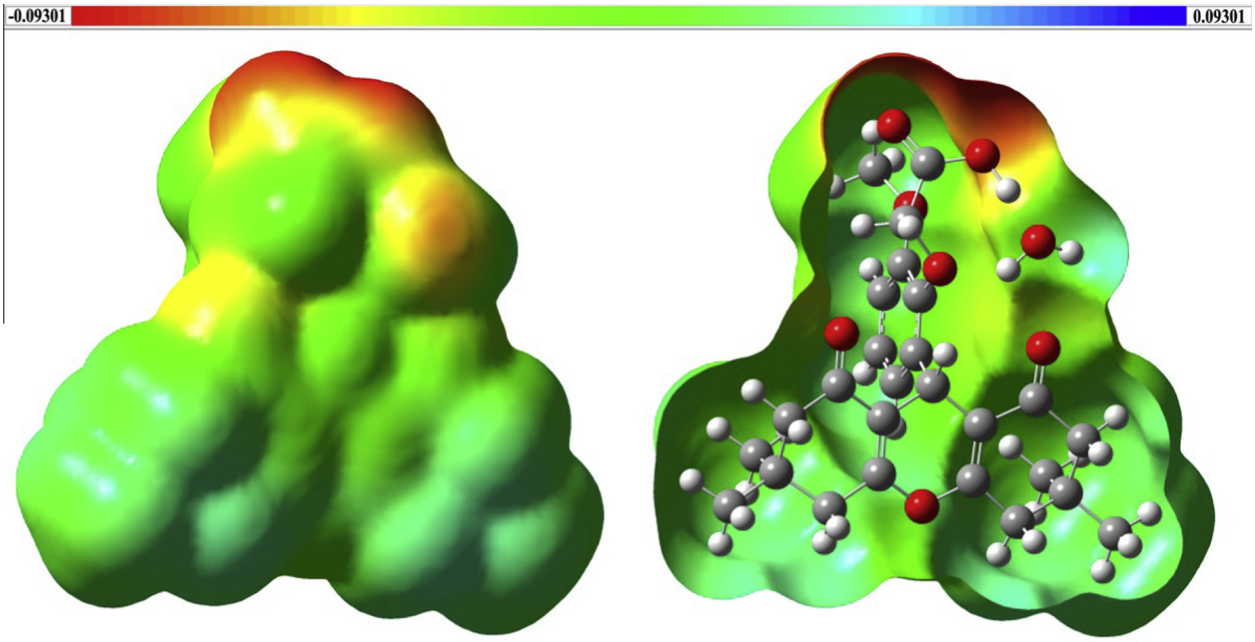

Fig. 7. Molecular Electrostatic Potential (MEP) of **2b·H$_2$O**.

Thus, Fig. 7 confirms the existence of an intermolecular O–H···O interaction. This was confirmed from the single crystal XRD studies (Fig. 3). The Molecular Electrostatic Potential map of **2b** (*vide* Supporting information) is nearly the same as that of **2b·H$_2$O** (Fig. 7). The maximum and minimum potential values are different for **2b** (−0.08276 to +0.08276 a.u) and **2b·H$_2$O** (−0.09301 to +0.09301 a.u). This further confirms that the presence of a water molecule increases the stability of **2b·H$_2$O**.

In the MEP of **2c** (*vide* Supporting information), the negative region (red) is located on the carbonyl oxygen atoms (O2, O3, and O5) with a minimum value of −0.07064 a.u, and the maximum positive region (blue) on carboxylic acid hydrogen atom (H6O) with a maximum value of 0.07064 a.u. This confirms the existence of an intermolecular O–H···O interaction. Fig. 4 reveals that the intermolecular H-bonding was observed in single crystal XRD. But in ester **5b**, the MEP (*vide* Supporting information) revealed the negative region (red) on carbonyl oxygen atoms (O2, O3, and O5) with a maximum value of −0.07047 a.u but no positive region (blue) was observed. This showed that there is no intermolecular dipole–dipole interaction and the molecule may be stabilized by short contacts. Single crystal XRD of **5b** also confirmed the presence of short contacts. Using the above data, the intermolecular interaction of **2a·H$_2$O** (no single crystal) was solved using MEP. Fig. 7 showed that **2a·H$_2$O** has similar type of MEP as that of **2b·H$_2$O**, excepting that the Molecular Electrostatic Potential energy is varied (−0.09163 to +0.09163 a.u).

3.5.2. Frontier molecular orbital analysis

We have investigated the electronic structures of the compounds **2a–c** and **5b** using DFT method [31]. The electron density of HOMO is the same for **2a**, **2c** and **5b** (Fig. 8). The electron density is mainly located on the phenyl ring with a little amount on the middle ring and the carbonyl group of other two rings of xanthene. But the electron density for **2b** is mainly located on the phenyl ring. The electron density of LUMO for **2a**, **2c**, and **5b** is located with the major portion on the middle ring and the carbonyl group of xanthene and a very little amount in phenyl ring whereas for **2b** that is present at the middle ring and the carbonyl group of xanthene part. Among the non-hydrated compounds **2a–c** and **5b**, compound **2b** has minimum HOMO–LUMO energy gap (4.19 eV). These results suggest that **2b** enjoys more stability than the other molecules.

The proposed reaction mechanism is also supported by energy minimization studies [32]. The HOMO–LUMO energy gap for the intermediates I, II, III, IV, and V (Fig. 1) are 3.0265, 6.2548, 5.7677, 6.3296, and 5.6877 eV respectively (*vide* Supporting information). These values indicate that when the reaction takes place, the ΔE increases for the formation of intermediate I to V as proposed in Fig. 1. The change in energy (4.6907 eV) is much significant in V which results in the formation of the final product, **2a**. The optimized structures of the intermediates III, IV, and V show the proton transfer from –COOH group to the corresponding nucleophilic site. This is also observed in the *para*- isomer (*vide*

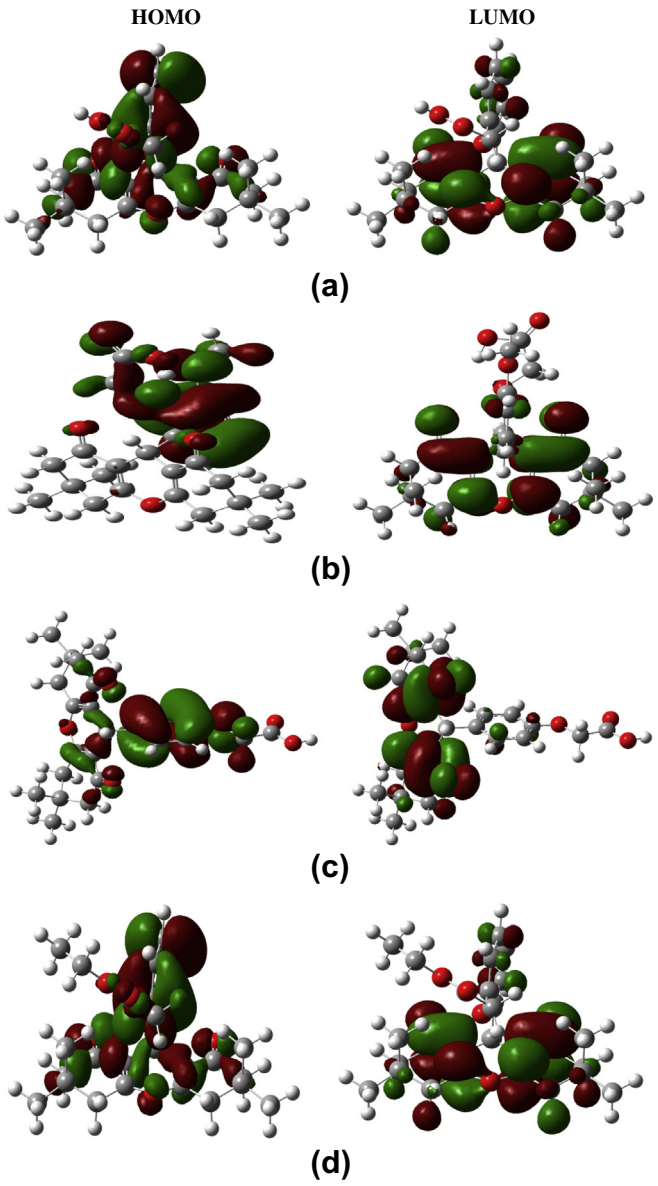

Fig. 8. HOMO–LUMO energy structures of (a) **2a**, (b) **2b**, (c) **2c**, and (d) **5b**.

Supporting information). This confirms the self catalyzed Bronsted–Lowry acid catalytic process.

The results from Table 5 show that **2c** has the highest energy gap, highest hardness and lowest softness; and **2b·H_2O** has the lowest energy gap, lowest hardness, and highest softness. Compound **5b** has the lowest nucleophilicity/electron accepting character. This is confirmed from DPPH radical scavenging activity (Table 2).

4. Conclusion

In summary, one-pot, in-water syntheses of phenoxyaliphatic acids of 1,8-dioxo-octahydroxanthene derived from dimedone and formylphenoxyaliphatic acids have been reported. We investigated the geometry and bonding nature of xanthene derivatives by single crystal X-ray technique. Xanthene **2b** is stabilized through intermolecular H-bonding with water molecules. Compound **2a** has better scavenging activity and antiproliferative effects on A431 cell line than other derivatives. Total energy, Molecular Electrostatic Potential map, and HOMO–LUMO results indicated that compounds, **2a** and **2b** stabilized by intermolecular hydrogen bonding with water molecules have the lowest values. Single crystal XRD and DFT studies confirmed that the hydrated *ortho* isomers are more stable. Experimental and theoretical results confirmed the proposed mechanistic aspects of the self-catalyzed syntheses of phenoxyaliphatic acid derivatives of 1,8-dioxo-octahydroxanthene.

Acknowledgements

Authors thank Dr. K. Ramalakshmi, Plantation Products Spices and Flavour Technology Department, Central Food Technological Research Institute, Council of Scientific and Industrial Research (CSIR), Mysore, India. One of the authors (G.S. Suresh Kumar) gratefully thanks Madurai Kamaraj University, Madurai, Tamilnadu, India and CDRI, Lucknow, India for spectral studies.

Appendix A. Supplementary material

Supplementary data associated with this article can be found, in the online version, at http://dx.doi.org/10.1016/j.molstruc.2013.11.016.

References

[1] (a) M. Orio, D.A. Pantazis, F. Neese, *Photosynth Res.* 102 (2009) 443;
(b) F.D. Proft, P. Geerlings, Chem. Rev. 101 (2001) 1451.
[2] M.E. Zandler, F. D'Souza, C.R. Chimie 9 (2006) 960.
[3] (a) J. Jeyakanthan, D. Velmurugan, Cryst. Res. Technol. 34 (1999) 1334;
(b) A. Domling, I. Ugi, Angew. Chem., Int. Ed. Engl. 39 (2000) 3168.
[4] (a) S.B. Krasnoff, D. Faloon, E. Williams, D.M. Gibson, Biocont. Sci. Tech. 9 (1999) 215;
(b) R.W. Lambert, J.A. Martin, J.H. Merrett, K.E.B. Parkes, G.J. Thomas, PCT Int. Appl. WO 9706178, Chem. Abstr. 126 (1997) 212377y;
(c) T. Hideo, Jpn. Tokkyo Koho JP 56005480, Chem. Abstr. 95 (1981) 80922b;
(d) J.P. Poupelin, G. Saint-Rut, O. Foussard-Blanpin, G. Narcisse, G. Uchida-Ernouf, R. Lacroix, Eur. J. Med. Chem. 13 (1978) 67.
[5] S.M. Menchen, S.C. Benson, J.Y.L. Lam, W. Zhen, D. Sun, B.B. Rosenblum, S.H. Khan, M. Taing, Chem. Abstr. 139 (2003) p54287f. U. S. Patent, US6583168;
(b) O. Sirkeeioglu, N. Talinli, A. Akar, J. Chem. Res. Synop. (1995) 502;
(c) M. Ahmad, T.A. King, B.H. Cha, J. Lee, J. Phys. D: Appl. Phys. 35 (2002) 1473.
[6] (a) V. Bala, Y.S. Chhonker, S.R. Hashim, Asian J. Chem. 22 (5) (2010) 3447;
(b) G.S. Suresh Kumar, P.G. Seethalakshmi, N. Bhuvanesh, S. Kumaresan, J. Mol. Str. 1034 (2013) 302;
(c) G.S. Suresh Kumar, P.G. Seethalakshmi, D. Sumathi, N. Bhuvanesh, S. Kumaresan, J. Mol. Str. 1035 (2013) 476;
(d) G.S. Suresh Kumar, P.G. Seethalakshmi, N. Bhuvanesh, S. Kumaresan, J. Mol. Str. 1050 (2013) 88.
[7] S. Marc-Olivier, L. Chao-Jun, Chem. Soc. Rev. 41 (2012) 1415.
[8] R.N. Butler, A.G. Coyne, Chem. Rev. 110 (2010) 6302.
[9] (a) H. Guang-Fan, C. Bin, C. Li-Zhuang, H. Xiao-Lei, J. Heterocyclic Chem. 49 (2012) 195;
(b) P.P. Salvi, A.M. Mandhare, A.S. Sartape, D.K. Pawar, S.H. Han, S.S. Kolekar, Comptes Rendus Cheimie 14 (2011) 883;
(c) F. Dong, Y. Jin-Ming, L. Zu-Liang, J. Heterocyclic Chem. 48 (2011) 468;
(d) W. Rui-Hua, C. Bin, Z. Wen-Tao, H. Guang-Fan, Synth. Comm. 40 (2010) 1867.
[10] B.S. Furniss, A.J. Hannaford, P.W.G. Smith, R. Austin, Vogel's Text book of Practical Organic Chemistry, fifth ed., Longman Scientific & Technical, 1989.
[11] (a) G.S. Suresh Kumar, S. Kumaresan, J. Chem. Sci. 124 (4) (2012) 857;
(b) G.S. Suresh Kumar, S. Kumaresan, Int. J. Curr. Chem. 3 (3 & 4) (2012) 91;
(c) G.S. Suresh Kumar, S. Kumaresan, C. Shiju, Bijoy Mohan Das, G. Anantharaj, S. Subramanian, Int. J. Basic Appl. Chem. Sci. 2 (2) (2012) 1.
[12] APEX2, Program for Data Collection on Area Detectors, BRUKER AXS Inc., 5465 East Cheryl Parkway, Madison, WI 53711–5373 USA.
[13] G.M. Sheldrick, SADABS, Program for Absorption Correction of Areadetector Frames, BRUKER AXS Inc., 5465 East Cheryl Parkway, Madison, WI 53711–5373, USA.
[14] (a) G.M. Sheldrick, Acta Cryst. A64 (2008) 112;
(b) XS, BRUKER AXS Inc., 5465 East Cheryl Parkway, Madison, WI USA, pp. 53711–5373.
[15] O.V. Dolomanov, L.J. Bourhis, R.J. Gildea, J.A.K. Howard, H. Puschmann, J. Appl. Cryst. 42 (2009) 339.
[16] A.L. Spek, J. Appl. Cryst. 36 (2003) 7.
[17] M.S. Blois, Nature 4617 (1958) 1199.
[18] (a) K. Ramalakshmi, G. Hithamani, K.R. Asha, L.J. Mohan Rao, Int. J. Food Sci. Technol. 46 (2011) 109;
(b) G.S. Suresh Kumar, S. Kumaresan, A. Antony Muthu Prabhu, P.G. Seethalakshmi, Spectrochim. Acta A 101 (2013) 254.

[19] (a) T. Mosmann, J. Immunol. Methods 65 (1983) 55;
(b) A. Monks, D. Scudiero, P. Skehan, R. Shoemaker, K. Paull, D. Vistica, C. Hose, J. Lonley, P. Cronise, A. Vaigro-Wolff, M. Gray-Goodrich, H. Cmpbell, J. Mayo, M. Boyd, J. Natl. Cancer Inst. 83 (1991) 757.
[20] (a) C. Lee, W. Yang, R.G. Parr, Phys. Rev. B 37 (1993) 5612;
(b) A.D. Becke, J. Chem. Phys. 98 (1993) 5648.
[21] M.J. Frisch, G.W. Trucks, H.B. Schlegel, G.E. Scuseria, M.A. Robb, J.R. Cheeseman, G. Scalmani, V. Barone, B. Mennucci, G.A. Petersson, H. Nakatsuji, M. Caricato, X. Li, H.P. Hratchian, A.F. Izmaylov, J. Bloino, G. Zheng, J.L. Sonnenberg, M. Hada, M. Ehara, K. Toyota, R. Fukuda, J. Hasegawa, M. Ishida, T. Nakajima, Y. Honda, O. Kitao, H. Nakai, T. Vreven, J.A. Montgomery Jr., J.E. Peralta, F. Ogliaro, M. Bearpark, J.J. Heyd, E. Brothers, K.N. Kudin, V.N. Staroverov, R. Kobayashi, J. Normand, K. Raghavachari, A. Rendell, J.C. Burant, S.S. Iyengar, J. Tomasi, M. Cossi, N. Rega, J.M. Millam, M. Klene, J. E. Knox, J.B. Cross, V. Bakken, C. Adamo, J. Jaramillo, R. Gomperts, R.E. Stratmann, O. Yazyev, A.J. Austin, R. Cammi, C. Pomelli, J.W. Ochterski, R.L. Martin, K. Morokuma, V.G. Zakrzewski, G.A. Voth, P. Salvador, J.J. Dannenberg, S. Dapprich, A.D. Daniels, O. Farkas, J.B. Foresman, J.V. Ortiz, J. Cioslowski, D.J. Fox, Gaussian Inc., Wallingford CT, 2009.
[22] (a) A. Antony Muthu Prabhu, N. Rajendiran, J. Fluore. 22 (2012) 1461;
(b) G.S. Suresh Kumar, A. Antony Muthu Prabhu, S. Jegan Jenniefer, N. Bhuvanesh, P. Thomas Muthiah, S. Kumaresan, J. Mol. Str. 1047 (2013) 109.
[23] A. Antony Muthu Prabhu, V.K. Subramanian, N. Rajendiran, Spectrochim. Acta 96A (2012) 95.
[24] (a) T. Sivasankar, A. Antony Muthu Prabhu, M. Karthick, N. Rajendiran, J. Mol. Stuct. 1028 (2012) 57;
(b) M. Jude Jenita, A. Antony Muthu Prabhu, N. Rajendiran, Ind. J. Chem. 51A (2012) 1686.
[25] M. Linder, T. Brinck, J. Org. Chem. 77 (2012) 6563.
[26] M. Bayat, H. Imanieh, S.H. Hossieni, Chinese Chem. Lett. 20 (2009) 656.
[27] (a) A. Corma, H. Garcia, Chem. Rev. 103 (2003) 4307;
(b) T. Akiyama, Chem. Rev. 107 (2007) 5744.
[28] (a) M.C. Etter, J.C. MacDonald, J. Bernstein, Acta Cryst. B46 (1990) 256;
(b) M.C. Etter, Acc. Chem. Res. 23 (1990) 120;
(c) J. Bernstein, R.E. Davis, L. Shimoni, N.L. Chang, Angew. Chem. Int. Ed. Engl. 34 (1995) 1555;
(d) M.C. Etter, J. Phys. Chem. 95 (1991) 4601.
[29] I. Coric, D. Milic, D.M. Calogovic, L. Tomaskovic, Struct. Chem. 20 (2009) 73.
[30] E. İnkaya, M. Dinçer, E. Şahan, İ. Yıldırım, Spectrochim. Acta A 114 (2013) 92.
[31] A.G. Al-Sehemi, A. Irfan, A.M. Fouda, Spectrochim. Acta A 111 (2013) 223.
[32] (a) I. Abulkalam Azath, P. Puthiaraj, K. Pitchumani, ACS Sustainable Chem. Eng. 1 (1) (2013) 174;
(b) R.S. Bertoa, F. Saliu, M. Bruschi, B. Rindone, Tetrahedron 68 (2012) 8267;
(c) G. Gayatri, G. Narahari Sastry, J. Chem. Sci. 117 (5) (2005) 573.